Discovery of several large families of Topological Insulator classes with backscattering-suppressed spin-polarized single-Dirac-cone on the surface

Su-Yang Xu,[1,2] L. A. Wray,[1] Y. Xia,[1] R. Shankar,[1] A. Petersen,[1] A. Fedorov,[3]
H. Lin,[4] A. Bansil,[4] Y. S. Hor,[5] D. Grauer,[5] R. J. Cava,[5] and M. Z. Hasan[1,2,6]

[1]*Joseph Henry Laboratory, Department of Physics,*
Princeton University, Princeton, New Jersey 08544, USA
[2]*Princeton Center for Complex Materials,*
Princeton University, Princeton, New Jersey 08544, USA
[3]*Lawrence Berkeley National Laboratory, Berkeley, California 94305, USA*
[4]*Department of Physics, Northeastern University,*
Boston, Massachusetts 02115, USA
[5]*Department of Chemistry, Princeton University,*
Princeton, New Jersey 08544, USA
[6]*Princeton Institute for Science and Technology of Advanced Materials,*
Princeton University, Princeton, New Jersey 08544, USA

PACS numbers:

Three dimensional topological insulators are novel states of quantum matter that feature spin-momentum locked helical Dirac fermions on their surfaces [1–13] and hold promise to open new vistas in spintronics, quantum computing and fundamental physics. Experimental realization of many of the predicted topological phenomena requires finding multi-variant topological band insulators which can be multiply connected to magnetic semiconductors and superconductors [7, 8, 10, 11, 14–23]. Here we present our theoretical prediction and experimental discovery of several new topological insulator classes in $AB_2X_4(124)$, $A_2B_2X_5(225)$, $MN_4X_7(147)$, $A_2X_2X'(221)$ [A,B=Pb,Ge,Sb,Bi and M,N=Pb,Bi and X,X'=Chalcogen family]. We observe that these materials feature gaps up to about 0.35eV. Multi-variant nature allows for diverse surface dispersion tunability, Fermi surface spin-vortex or textured configurations and spin-dependent electronic interference signaling novel quantum transport processes on the surfaces of these materials. Our discovery also provides several new platforms to search for topological-superconductivity in these exotic materials.

The crystal structures of AB_2X_4, $A_2B_2X_5$, and MN_4X_7 are composed of X layers forming a cubic close packing, with a fraction of octahedral interstices occupied by A and B atoms [24] (Fig.1). The unit cell of AB_2X_4 is formed by stacking three 7-atomic-layer-slabs in the sequence X(1)-B-X(2)-A-X(2)-B-X(1) together [24]. We present our first-principle theoretical calculations of the (111) surface electronic structure of AB_2X_4, $A_2B_2X_5$, MN_4X_7, A_2X_2X' respectively, along the $\bar{K} - \bar{\Gamma} - \bar{M}$ momentum-space trajectories. Results reveal a singly degenerate gapless surface state Dirac cone centered at the $\bar{\Gamma}$ point for $PbSb_2Te_4$, $PbBi_2Se_4$, $GeBi_2Te_4$, $Pb_2Bi_2Se_5$, $PbBi_4Te_7$, Sb_2Te_2Se, Bi_2Se_2S, and Sb_2Te_2S (see online Supplementary Information (SI) for the rest), indicating that these materials belong to the $Z_2 = -1$ topological insulator class. It is interesting to note that crystals of MN_4X_7, although possessing bulk inversion symmetry, can feature two possible surface terminations along the (111) direction (labeled I and II in Fig. 1f). In our calculations these two variants of the $PbBi_4Te_7$ (111) surface possesses distinct band dispersions and anisotropy. A significantly greater charge density is expected in the top atomic layers of surface II by comparison with surface I, suggesting that the application of a Coulomb potential gradient during evaporative growth or cleavage can generate the desired surface or an alloyed combination of the two. By contrast, a fully gapped system without any surface state is observed in $GeSb_2Te_4$. We hence predict

that $GeSb_2Te_4$ is topologically trivial at its experimental lattice constants. Our theoretical results show a wide range of variability in electronic and spin properties among these materials. The theoretical bulk band gap varies over an order of magnitude from $0.01eV$ to $0.31eV$ (experimental band-gaps are larger, see below). The topological surface electron kinetics range from a nearly isotropic Dirac cone (e.g. $PbBi_2Se_4$) to strongly anisotropic (hexagonal warping etc.) and doping-dependent electron kinematics on the $PbBi_4Te_7$ surface I.

We have grown several of these materials in their single crystal forms. We present experimental results on a few representative compounds (the rest will be presented elsewhere) that exhibit the clearest surface features: $GeBi_2Te_4$(GBT124), Bi_2Te_2Se(BTS221) and Sb_2Te_2Se(STS221) are the focus of this paper. The bulk crystal symmetry fixes a hexagonal Brillouin zone (BZ) for the cleaved (111) surface (Fig. 2a) on which $\bar{\Gamma}$ and $\bar{M}$ are the time reversal invariant momenta (TRIM) at which Dirac points or Kramers' nodes can occur. Band structure measurements using angle-resolved photoemission spectroscopy are presented by scanning over the full BZ. High resolution dispersion maps along $\bar{\Gamma} - \bar{M}$ and $\bar{\Gamma} - \bar{K}$ directions trace a clear single Dirac cone for GBT124 and BTS221 (Fig. 2b). The Dirac bands intersect at the Fermi level at $0.14\mathring{A}$, with a particle velocity of $3.6\times10^5 m/s$ along $\bar{\Gamma} - \bar{M}$ and cross E_F at $0.12\mathring{A}$ along $\bar{\Gamma} - \bar{K}$ with a much higher velocity of $5.0\times10^5 m/s$. No other band feature is observed inside the Dirac cone, suggesting that the bulk conduction band minimum is above the chemical potential and the naturally occurring Fermi level lies inside the band-gap.

Other members of the family such as BTS221 and STS221 are also single Dirac cone topological insulators. Incident photon energy dependence (Fig. 4b) on BTS221 clearly verifies the surface origin of the "V" shaped Dirac band since it does not show any k_z dispersion with incident photon energy. Band structure below the Dirac point, however, is found to change dramatically with k_z, indicating that it represents the bulk bands. Potassium surface deposition is performed in order to image the Dirac point of STS221. With 1.67 $\mathring{A}$ of K deposition, the lower Dirac cone bands are observed to cross each other (Fig. 4c). Therefore, we report STS221 as the first naturally p-type topological insulator to be experimentally confirmed. Remarkably in BTS221 we observe a Fermi momentum and velocity of $0.09\mathring{A}$ and $1.1\times10^6 m/s$ along $\bar{\Gamma} - \bar{M}$, and $0.08\mathring{A}$ and $1.5\times10^6 m/s$ along $\bar{\Gamma} - \bar{K}$. This is nearly a factor of three larger than the Fermi velocity in any other known topological insulator.

While the spin-textured Dirac states guarantee a non-zero surface Berry's phase, warping

effects observed on the surface suggest three dimensional spin-textures [26]. Spin-texture determines the detailed nature of surface charge transport, since on the topological surface spin and quasiparticle momentum are locked in relative to one another. In general, deviations from the ideal Dirac cone shape of the surface states lead to three dimensional topological spin-textures. In order to systematically analyze the surface band structure and warping of GBT124, and how it could be tuned with bulk doping, we perform a series of high resolution ARPES measurements of the constant energy contours at different binding energies (Fig. 3a, b). The Fermi contour of GBT124 (constant energy contour at $E_B = 0.01eV$, see Fig. 3a) is warped, demonstrating the hexagonal warping effect [25]. When the binding energy is increased from the Fermi level, the effect of the bulk potential vanishes and the shape of the contour recovers to a circle (Fig. 3b). Lowering the binding energy further results in a Fermi surface of a single Dirac point with no other features. Hence unlike Bi_2Te_3 whose Dirac point is buried under portions of the lower surface Dirac band and the bulk valence band maximum [6, 9], GBT124 has an isolated Dirac point, which makes it possible to bring the system into a Dirac point transport regime [8] not possible in Bi_2Te_3. Constant energy contours below the Dirac point are observed to consist of the lower cone, with an additional six-fold symmetric feature extending outside along all $\bar{\Gamma} - \bar{M}$ directions.

The unique spin-helical Dirac fermions of topological insulators embody a momentum-locked spin polarization that strongly affects electron dynamics, and is characterized by a non-trivial topological Berry's phase as demonstrated by us previously [4, 8]. The spin texture of GBT124 around the hexagonal Fermi contour in three dimensional space. Spin is found to develop a large out-of-plane σ_z component which results from the hexagonal warping effect due to the bulk crystal potential. The in-plane spin component, on the other hand, follows the Fermi contour with *left-handed chirality* and thus achieves a quantum phase of π. A full 3-D image of the topological surface Dirac band with the spin z-component suggests that the out-of-plane spin in GBT124 is found to oscillate around the constant energy contour with a period of $2\pi/3$.

Our comprehensive experimental measurements of the constant energy contours along with the spin-texture observations above will help gain key insights on the quasiparticle interference and scattering processes relevant for surface transport. These experimental realizations of topological insulators reveal rich interplay of electronic, spin, quasiparticle interference and potential ordering instabilities on the topological surface in their native

state. These ternaries also hold promise for observing superconductivity in doped topological insulators [10].

[1] Hasan, M. Z. & Kane, C. L. Topological Insulators. arXiv:1002.3895 Rev. of Mod. Phys. (in press) (2010).

[2] Moore, J. E. The birth of topological insulators. *Nature* **464**, 194 (2010); Zhang, S. -C. Topological states of quantum matter. *Physics* **1**, 6 (2008); X.-L. Qi and S.-C. Zhang, Quantum Spin Hall effect and Topological Insulators *Physics Today* **63**, 33 (2010).

[3] Hsieh, D. *et al.* A topological Dirac insulator in a quantum spin Hall phase. *Nature* **452**, 970 (2008).

[4] Hsieh, D. *et al.* Observation of unconventional quantum spin textures in topological insulators. *Science* **323**, 919 (2009).

[5] Xia, Y. *et al.* Observation of a large-gap topological-insulator class with a single Dirac cone on the surface. *Nature Physics* **5**, 398 (2009). Also see, arXiv:0812.2078v1 (2008).

[6] Hsieh D. *et al.* Observation of Time-Reversal-Protected Single-Dirac-Cone Topological-Insulator States in Bi_2Te_3 and Sb_2Te_3. *Phys. Rev. Lett.* **103**, 146401 (2009).

[7] Hor, Y. S. *et al.* p-type Bi_2Se_3 for topological insulator and low-temperature thermoelectric applications. *Phys. Rev. B* **79**, 195208 (2009).

[8] Hsieh, D. *et al.* A tunable topological insulator in the spin helical Dirac transport regime. *Nature* **460**, 27 (2009).

[9] Chen, Y. L. *et al.* Experimental Realization of a Three-Dimensional Topological Insulator, Bi_2Te_3. *Science* **325**, 178 (2009).

[10] Wray, L. A. *et al.* Observation of unconventional band topology in a superconducting doped topological insulator, $Cu_xBi_2Se_3$: Topological Superconductor or non-Abelian superconductor? arXiv:0912.3341v1 (2009).

[11] Hor, Y. S. *et al.* Development of ferromagnetism in the doped topological insulator $Bi_{2-x}Mn_xTe_3$. *Phys. Rev. B* **81**, 195203 (2010).

[12] Fu, L., Kane, C. L. & Mele, E. J. Topological Insulators in Three Dimensions. *Phys. Rev. Lett.* **98**, 106803 (2007).

[13] Moore, J. E. & Balents, L. Topological invariants of time-reversal-invariant band structures.

Phys. Rev. B **75**, 121306(R) (2007).

[14] Roy, R. Topological phases and the quantum spin Hall effect in three dimensions. *Phys. Rev. B* **79**, 195322 (2009).

[15] Qi, X. -L. *et al.* Topological field theory of time-reversal invariant insulators. *Phys. Rev. B* **78**, 195424 (2008).

[16] Fu, L. & Kane, C. L. Probing Neutral Majorana Fermion Edge Modes with Charge Transport. *Phys. Rev. Lett.* **102**, 216403 (2009).

[17] Essin A., Moore J. E. & Vanderbilt D. Magnetoelectric polarizability and axion electrodynamics in crystalline insulators. *Phys. Rev. Lett.* **102**, 146805 (2009).

[18] Qi, X. -L. *et al.* Inducing a magnetic monopole with topological surface states. *Science* **323**, 1184 (2009).

[19] Dzero, M. *et al.* Topological Kondo insulator. *Phys. Rev. Lett.* **104**, 106408 (2010).

[20] Linder, J. *et al.* Unconventional superconductivity on a topological insulator. *Phys. Rev. Lett.* **104**, 067001 (2010).

[21] Franz, M. Topological insulators: Starting a new family. *Nature Mater.* doi:10.1038/nmat2783 (2010).

[22] Lin, H. *et al.* Half-Heusler ternary compounds as new multifunctional experimental platforms for topological quantum phenomena. *Nature Mater.* doi:10.1038/nmat2771 (2010).

[23] Chadov, S. *et al.* Tunable multifunctional topological insulators in ternary Heusler compounds. *Nature Mater.* doi:10.1038/nmat2770 (2010).

[24] Agaev, K. A. & Semiletov S. A. Electron-diffraction study of the Bi_2GeTe_4 structure. *Kristallografiya* **10**, 109 (1965).

[25] Fu, L. Hexagonal Warping Effects in the Surface States of the Topological Insulator Bi_2Te_3. *Phys. Rev. Lett.* **103**, 266801 (2009).

[26] Hasan, M. Z., Lin, H. & Bansil, A. Warping the cone on a Topological Insulator. *Physics* **2**, 109 (2009).

[27] Xia, Y. *et al.* Topological Control: Systematic control of topological insulator Dirac fermion density on the surface of Bi_2Te_3. arXiv:0907.3089v1 (2009).

[28] Roushan, P. *et al.* Topological surface states protected from backscattering by chiral spin texture. *Nature* **460**, 1106 (2009).

[29] Hsieh, D. First observation of spin-helical Dirac fermions and topological phases in undoped

and doped Bi_2Te_3 demonstrated by spin-ARPES spectroscopy. arXiv:0904.12601v1 (2009).

[30] Blaha, P. *et al.* WIEN2k, An Augmented Plane Wave Plus Local Orbital Program for Calculating Crystal Properties. (2001).

[31] Perdew, J. P., Burke K. & Ernzerhof M. Generalized gradient approximation made simple *Phys. Rev. Lett.* **77**, 3865 (1996).

[32] Wang G., & Cagin T., Electronic structure of the thermoelectric materials Bi_2Te_3 and Sb_2Te_3 from first-principles calculations *Phys. Rev. B* **76**, 075201 (2007).
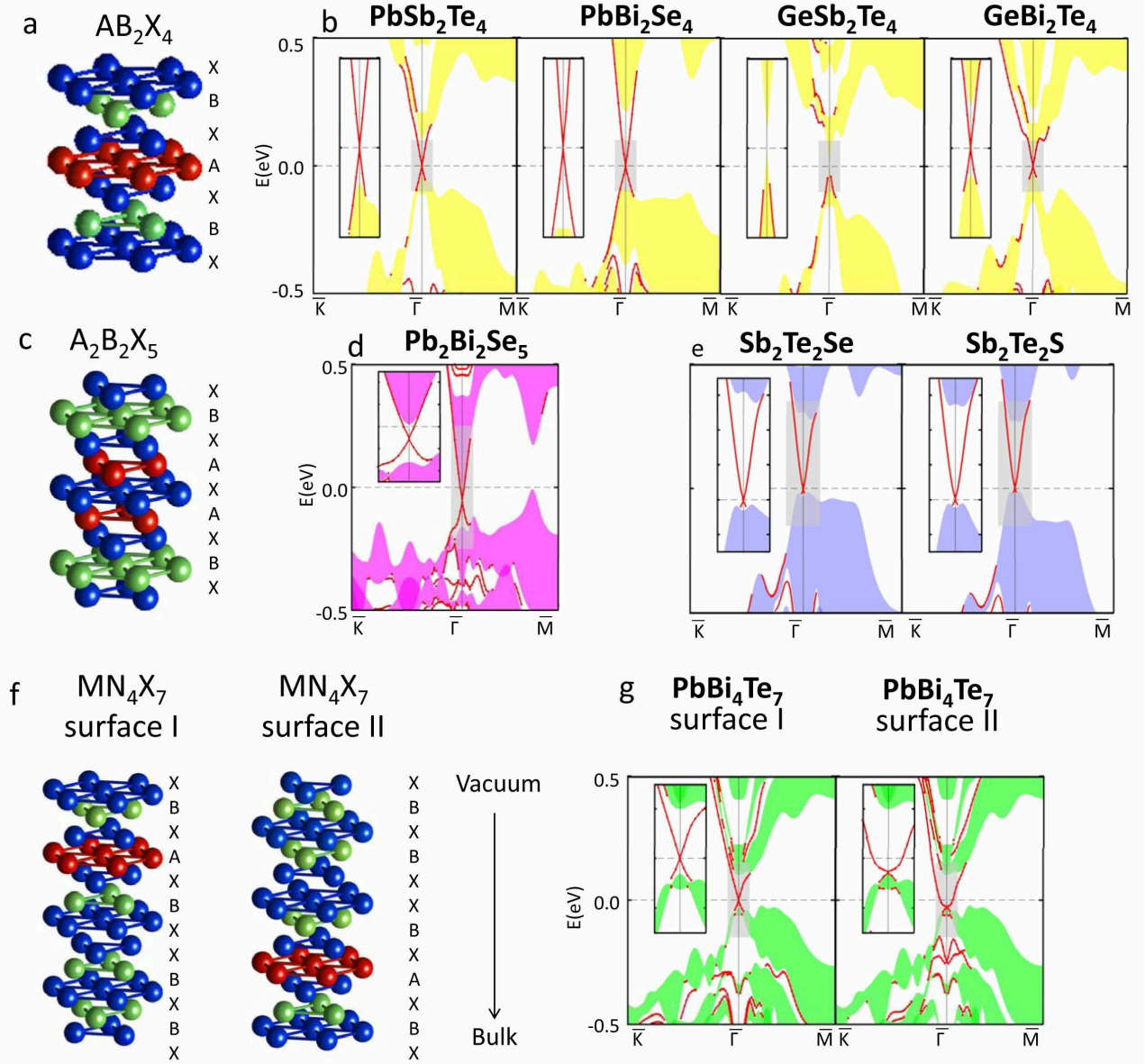
FIG. 1: **Topological insulator states in AB_2X_4, $A_2B_2X_5$, MN_4X_7, A_2X_2X' ternary compounds.** **a**, Crystal structure of AB_2X_4. AB_2X_4 crystal is made up of stacked 7-layer-slabs. **b**, First principle theoretical calculation of $PbSb_2Te_4$, $PbBi_2Se_4$, $GeSb_2Te_4$, and $GeBi_2Te_4$ respectively. Bulk band projections are represented by shaded areas. A single gapless surface band is observed in $PbSb_2Te_4$, $GeBi_2Te_4$ and $PbBi_2Se_4$. These results prove that $PbSb_2Te_4$, $GeBi_2Te_4$ and $PbBi_2Se_4$ belong to the $Z_2 = -1$ topological class. A fully gapped system is observed in $GeSb_2Te_4$, which indicates that $GeSb_2Te_4$ is topologically trivial. **c**, Crystal structure of $A_2B_2X_5$. **d-e**, First principle calculation of $Pb_2Bi_2Se_5$, Sb_2Te_2S and Sb_2Te_2S reveals $Z_2 = -1$ topological order. **f**, Crystal structure and two kinds of surface termination of MN_4X_7. **g**, Calculated bulk and surface electronic structure of $PbBi_4Te_7$ for each surface termination.
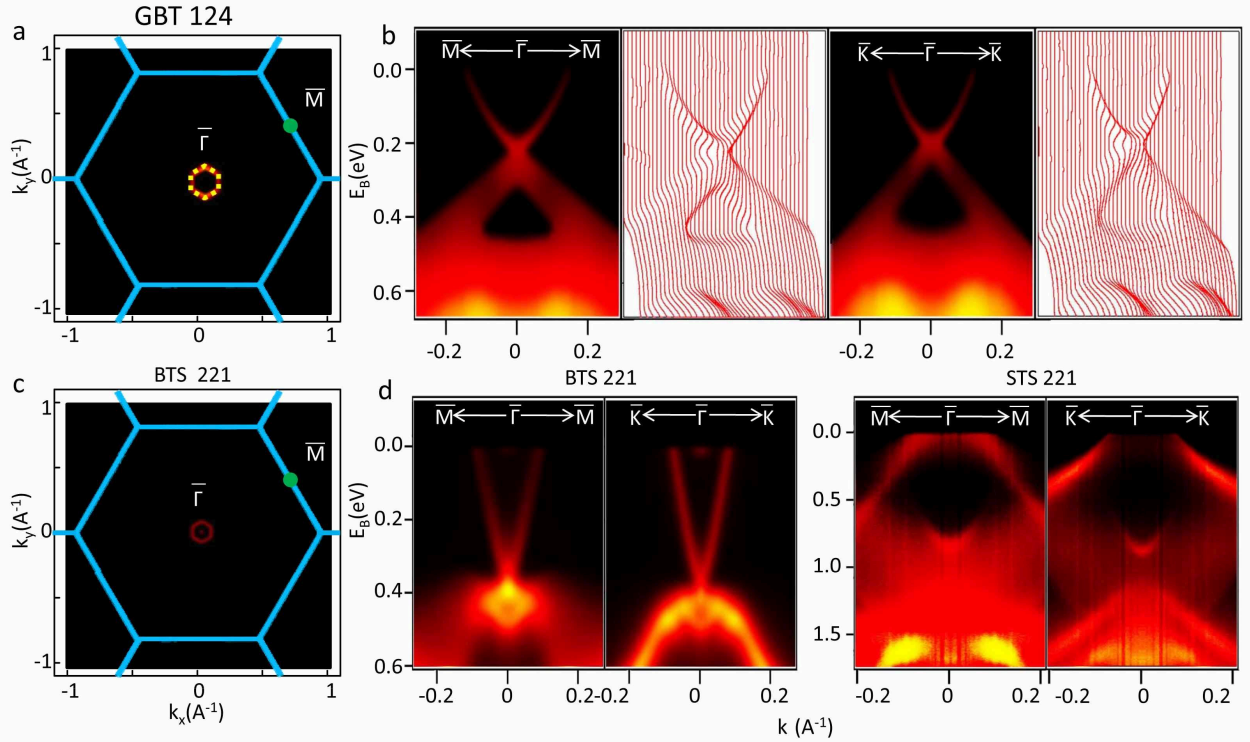
FIG. 2: **Long life time surface states in GBT124 and BTS221**: **a**, ARPES measurement over the First BZ on GBT124. **b**, High resolution ARPES measurements of band dispersion with the corresponding energy distribution curves along $\bar{\Gamma} - \bar{M}$ and $\bar{\Gamma} - \bar{K}$ directions. **c**. ARPES measurement over the First BZ on BTS221. **d**. High resolution ARPES measurements of band dispersion in BTS221 and STS221.
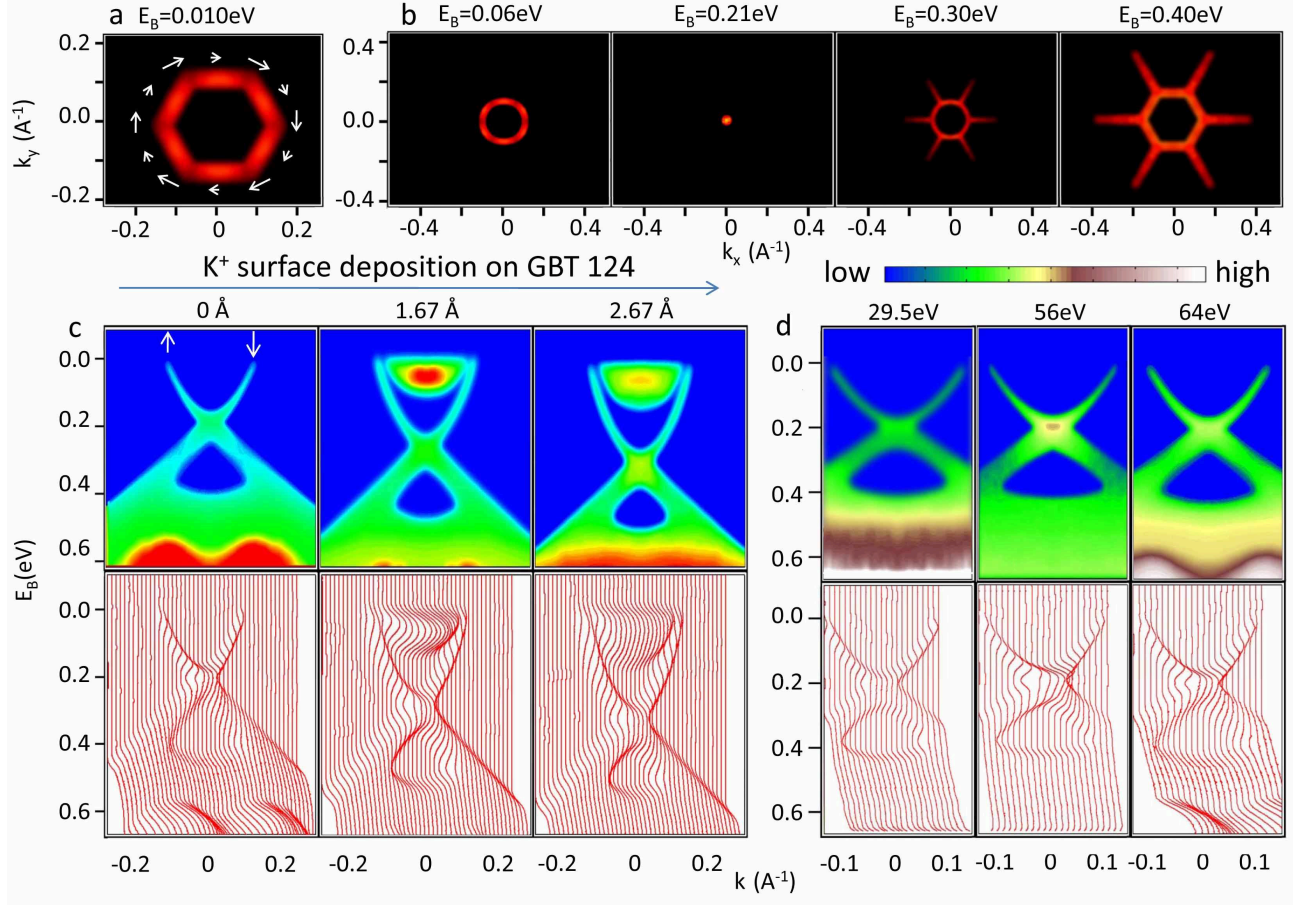
FIG. 3: **Evolution of topology through the Dirac node**: **a-b**, High resolution ARPES measurements of GBT124 constant energy contours at different binding energies. In-plane spin texture from the theoretical calculation is drawn on **a**. **c**, ARPES measurement of GBT124 $\bar{\Gamma} - \bar{K}$ band structure as potassium is deposited. Average thickness of the deposition layer is indicated on the top of each panel. **d**, Incident photon energy dependence of measurements along the $\bar{\Gamma} - \bar{K}$ direction. No k_z dispersion is observed, which confirms the surface character of the Dirac cone of a topological insulator.
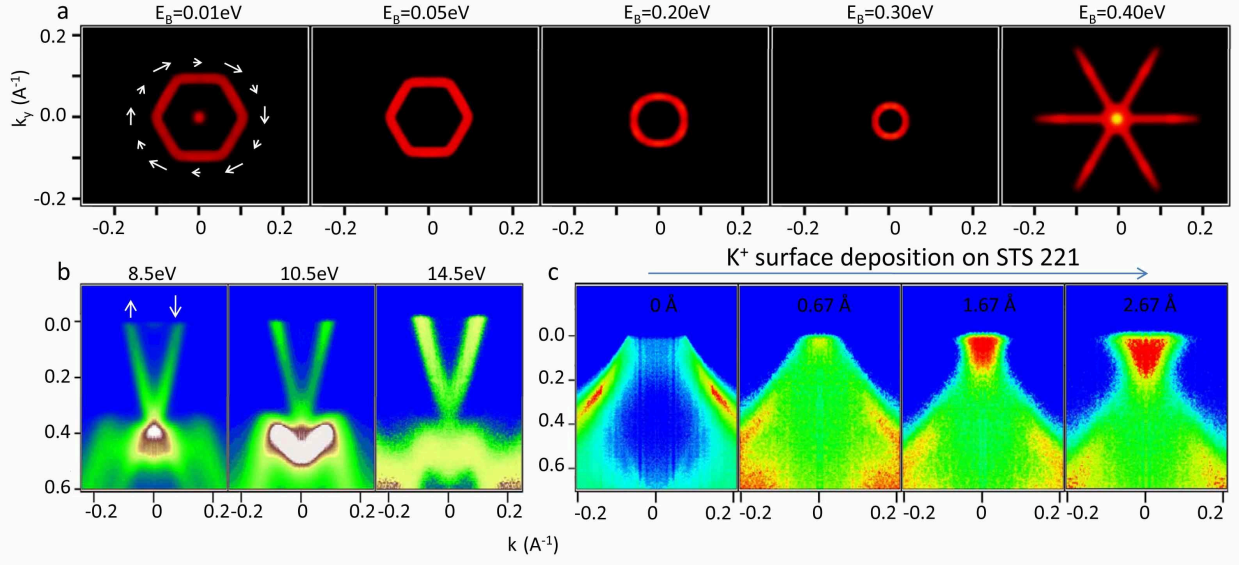
FIG. 4: **Warping evolution of topological states** **a**, High resolution ARPES measurements of constant energy contours on BTS221 at different binding energies. In-plane spin texture from the theoretical calculation is drawn on the first panel. **b**, Incident photon energy dependence of measurements along the $\bar{\Gamma} - \bar{M}$ direction on BTS221. No k_z dispersion of the "V" shaped Dirac band is observed, which confirms the surface character of the Dirac cone of a topological insulator. **c**, ARPES measurement of STS221 $\bar{\Gamma} - \bar{K}$ band structure as potassium is deposited. Average thickness of the deposition layer is indicated on the top of each panel.